AIP Advances ARTICLE pubs.aip.org/aip/adv

# Deposition of nanoparticles through a cylindrical tube of human respiratory system

Cite as: AIP Advances 14, 125320 (2024); doi: 10.1063/5.0239676
Submitted: 27 September 2024 • Accepted: 30 November 2024 •
Published Online: 17 December 2024

View Online Export Citation CrossMark

Mst. Sathi Akter,[1,2,a)] Mahtab U. Ahmmed,[1] Nilufer Yesmin Tanisa,[3] and Shakib Hossain[1]

## AFFILIATIONS

[1] Department of Mathematics, Jahangirnagar University, Dhaka 1342, Bangladesh
[2] Department of Mathematics, Uttara University, Dhaka 1230, Bangladesh
[3] Department of Physics, Uttara University, Dhaka 1230, Bangladesh

[a)] Author to whom correspondence should be addressed: sathiakter@uttarauniversity.edu.bd

## ABSTRACT

This paper proposes a mathematical model for nanoparticle deposition in the respiratory bronchiole of the human lung airways. The length of the respiratory bronchiole of the human lung is 1.2 mm, and the diameter is 0.5 mm. Therefore, to investigate the impact of inhaled nanoparticles within the lung bronchioles, first, we used the Navier–Stokes equation by including the Darcy term together with Newton's equation of motion. Then we non-dimensionalized the governing equation, and numerical solutions are obtained using the finite difference technique. Under the assumption of laminar pulsatile flow conditions and axial symmetry, the problem is simplified to a two-dimensional computational domain. The computational framework is implemented using MATLAB R2018 through user-defined code. Velocity propagation, the Reynolds number, and the Darcy number effect are performed to examine the flow conditions inside the respiratory bronchioles.



## NOMENCLATURE

| | |
|---|---|
| $a_0$ | Amplitude |
| $D_a$ | Darcy number |
| $d_p$ | Aerodynamic diameter |
| $\varepsilon$ | Media porosity |
| $f$ | Pulse rate |
| K | Permeability of parenchyma |
| $k_f$ | Stokes resistance coefficient |
| $p_l$ | Particle load |
| Re | Reynolds number |
| t | Time |
| $u_x$ | The velocity of air particles in the radial direction |
| $u_y$ | Air particles velocity in axial direction |
| $v_x$ | The velocity of dust particles in the radial direction |
| $v_y$ | Dust particles velocity in axial direction |
| $\mu$ | Dynamic viscosity |
| $\nu$ | Kinematic viscosity |
| $\rho_a$ | Density of air particles |
| $\rho_p$ | Density of dust particles |

## I. INTRODUCTION

Air pollution is becoming a more and more significant issue. Humans inhale billions of particles from the surrounding air every day.[1,2] In the human lung system, biological and other factors like breathing rhythm, particle characteristics, and deposition mechanisms affect airflow and particle transport. Different sizes of particles may reach different positions in the human body. Particles between 0.1 and 10 $\mu$m in diameter deposit differently depending on the flow rate from the mouth to the oropharynx.[3,4] Particles in the 10–20 $\mu$m range are likely to accumulate in the nasal cavity.[5] Extra thoracic space contains particles ranging in size from 4.9 to 44.3 $\mu$m (that is, in the nasal and oral airways, as well as the head and throat).[6] Experimental methods commonly used include *in vitro* models (e.g., lung-on-a-chip systems), *in vivo* animal models, and human studies with computational simulations to predict deposition patterns. Techniques like particle counters, impactors, and imaging methods (e.g., electron microscopy) enable precise measurement and visualization of deposition patterns.[7] Studied the most critical parameters for particle lung deposition measurements with a particular focus on nano-sized particles (here diameter <300 nm) to guide for measuring the lung deposition of inhaled nanoparticles, to facilitate comparison and harmonization of data, and to improve the quality of future particle lung deposition measurements.[8] Investigated the binding and uptake of nanoparticles by alveolar macrophages using flow cytometry analysis and confocal laser scanning microscopy.[9] Researched the nanoparticle (physicochemical) properties with toxicological pathways and cellular uptake mechanisms, sufficient and appropriate information for risk assessment and societal acceptance of nanomaterials and products made using nanotechnology.[10] studied the previous experimental investigations by also including aerosols other than ETS (diesel and petrol emissions).[10] They aimed to test and interpret the findings against current theoretical models of lung deposition.

Due to their minuscule size and incredibly high surface area-to-volume ratio, nanoparticles pose a serious risk to human respiratory health.[11] Researched the toxicity of nanoparticles by inhalation with great emphasis on the transport and deposition of nanoparticles in the respiratory system. In addition,[12–19] researchers showed numerical simulations for the deposition of nanoparticles. These studies focus on the nasal or oral airways and the upper tracheobronchial airways (from the trachea to generation G6). Recently[20] investigated the deposition of 100 nm-diameter nanoparticles and found that these particles eventually deposit in the alveolar ducts of the human lung after entering the lung more deeply. In addition, the impact of the Darcy number, porosity, and Reynolds number of air and particles inside the permeable alveolar duct has been shown by Kori and Pratibha.[21]

From above, we found that several research works have investigated the effects of lung nanoparticle deposition. Though Kori and Pratibha[21] and Saini *et al.*[20] investigated the alveolar duct, we have studied the respiratory bronchiole. Understanding the effects of nanoparticles on the lung and investigating the respiratory bronchiole's flow characteristics are the reasons behind this work.

Based on experimental results, a mathematical model was created to quantitatively characterize the movement and deposition of nanoparticles. These days, understanding the characteristics of pulmonary airflow in the human lung from the vast central bronchial airways to the acinar areas requires the use of computational fluid dynamics, or CFD. Therefore, to determine the effect of inhaled nanoparticles inside the respiratory bronchiole, we used the Navier–Stokes equation. The air and dust particle velocities are analyzed under several significant parameters, including the Reynolds number, the Darcy number, and the media porosity.

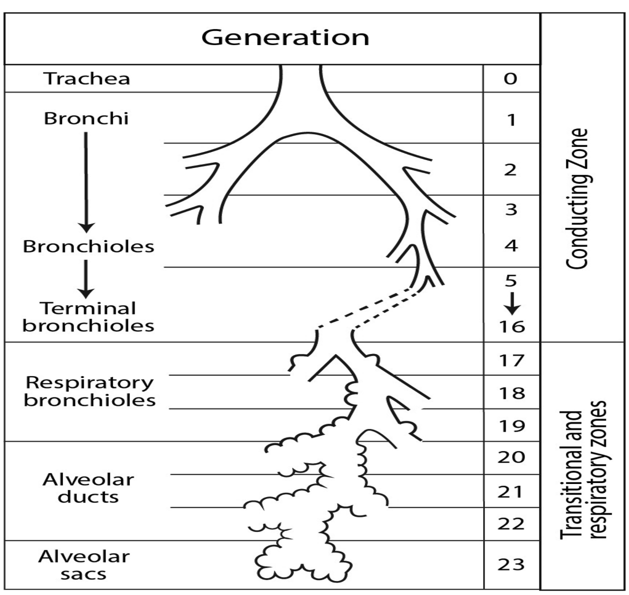


**FIG. 1.** Idealized human airway configuration.

## II. METHODS AND METHODOLOGY

### A. Respiratory airways and configuration

Air enters the trachea through the nose or mouth during inhalation. As seen in Fig. 1, it then travels via the respiratory system's bronchial tubes. To illustrate the flow of air through the respiratory bronchioles, a horizontal cylindrical tube of length 1.2 mm and diameter 0.5 mm is considered. We assume the radius of the cylinder is R, and it is assumed that the flow is perpendicular to the radius, which is shown in Fig. 2, where $x$ and $y$ are the axial and radial directions, respectively.

### B. Mathematical modeling of the governing equations

The human lung has its 23rd generation. Each subsequent generation looks like a cylindrical shape and is a smaller duplicate of the parent. The cylindrical tube's axis is traversed by an incompressible, fully developed laminar Newtonian fluid that is driven by a time-dependent sinusoidal pressure gradient. Saini *et al.* proposed a mathematical model,[20] which includes, due to the lung's porosity, the Darcy term is used to determine the velocity of propagation and the harmful effects of nanoparticles on the lung. Based on these presumptions, the fluid flow equations involving solid particles can be expressed in the cylindrical system $(r, z, t)$.

Equation of continuity for air particles,

$$\frac{\partial u_r}{\partial r} + \frac{u_r}{r} + \frac{\partial u_z}{\partial z} = 0. \quad (1)$$

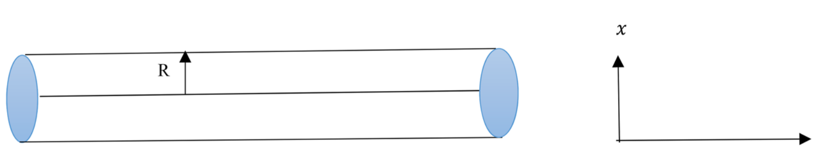


**FIG. 2.** The cylindrical shape of the bronchial tube.

Equation of continuity for dust particles,

$$\frac{\partial v_r}{\partial r} + \frac{v_r}{r} + \frac{\partial v_z}{\partial z} = 0. \tag{2}$$

Axial momentum equation for air particles,

$$\frac{\partial u_z}{\partial t} + \frac{u_r}{\varepsilon}\frac{\partial u_z}{\partial r} + \frac{u_z}{\varepsilon}\frac{\partial u_z}{\partial z} = -\frac{\varepsilon}{\rho_a}\frac{\partial P}{\partial z} + \upsilon\left(\frac{\partial^2 u_z}{\partial r^2} + \frac{1}{r}\frac{\partial u_z}{\partial r} + \frac{\partial^2 u_z}{\partial z^2}\right) + \left(-\frac{\varepsilon\upsilon}{K}u_r + k_f\frac{\rho_p}{\rho_a}(v_z - u_z)\right). \tag{3}$$

Axial momentum equation for dust particles,

$$\frac{\partial v_z}{\partial t} + v_z\frac{\partial v_z}{\partial z} + v_r\frac{\partial v_z}{\partial r} = \frac{k_f(u_z - v_z)}{m}, \tag{4}$$

where the radial and axial velocity components of air particles are $u_r(r,z,t)$, $u_z(r,z,t)$ and $v_r(r,z,t)$, $v_z(r,z,t)$ represent the radial and axial velocity components of dust particles, respectively. $K$ is permeability described by Ergun[22] as follows, and it is dependent upon media porosity $(\varepsilon)$,[23]

$$K = \frac{\varepsilon^3 {d_p}^2}{150(1-\varepsilon)^2}.$$

The following is our assumption on the time-dependent pressure gradient inside the respiratory bronchioles:

$$-\frac{\partial p}{\partial z} = a_0 \sin \omega t, \quad \omega = 2\pi f,$$

where $f$ is the pulse rate and $a_0$ is the amplitude.

For spherical particles, the Stokes resistance coefficient $(k_f)$ is $3\pi\mu d_p$. The coefficient of viscosity of air is $\mu$, and the diameter of dust particles is $d_p$.

### C. Non-dimensional form of the governing equations

The non-dimensional quantities are

$$u_x = \frac{u_r}{u_0}, u_y = \frac{u_z}{u_0}, v_x = \frac{v_r}{u_0}, v_y = \frac{v_z}{u_0}, x = \frac{r}{R}, y = \frac{z}{R}, p = \frac{P}{\rho_a {u_0}^2},$$
$$\tau = \frac{t u_0}{R}, D_a = \frac{K}{R^2}, P_l = \frac{\rho_p}{\rho_a}, S_m = \frac{R k_f}{u_0}, Re = \frac{R u_0}{\upsilon}.$$

On introducing the non-dimensional quantities, (1) and (2) become

$$\frac{\partial u_x}{\partial x} + \frac{u_x}{x} + \frac{\partial u_y}{\partial y} = 0, \tag{5}$$

$$\frac{\partial v_x}{\partial x} + \frac{v_x}{x} + \frac{\partial v_y}{\partial y} = 0. \tag{6}$$

Equation (3) becomes

$$\frac{\partial u_y}{\partial \tau} + \frac{u_x}{\varepsilon}\frac{\partial u_y}{\partial x} + \frac{u_y}{\varepsilon}\frac{\partial u_y}{\partial y} = -\varepsilon\frac{\partial p}{\partial y} + \frac{1}{Re}\left[\frac{\partial^2 u_y}{\partial x^2} + \frac{1}{x}\frac{\partial u_y}{\partial x} + \frac{\partial^2 u_y}{\partial y^2}\right] + \left(-\frac{\varepsilon}{D_a Re}u_x + S_m p_l(v_y - u_y)\right). \tag{7}$$

Equation (4) becomes

$$\frac{\partial v_y}{\partial \tau} + v_y\frac{\partial v_y}{\partial y} + v_x\frac{\partial v_y}{\partial x} = \frac{S_m(u_y - v_y)}{m}. \tag{8}$$

### D. Numerical scheme

For all spatial derivatives, we have used central difference approximations, and for the temporal derivative, we have used forward difference approximations. We have chosen $\Delta\tau = 4\times 10^{-6}$, $\Delta y = 0.006$, and $\Delta x = 0.003$ as the grid spacing for a $151 \times 201$ grid size for 0.008 seconds with 2000 nodes for time. Equations are then solved numerically using these results. The axial velocity discretization $u_y(x,y,\tau)$ is written as $u_y(x_i, y_j, \tau^n)$ or $(u_y)^n_{i,j}$. We define

$$x_i = i\Delta x; \qquad i = 0,1,2,3,\ldots, \mathrm{N},$$

$$y_j = j\Delta y; \qquad j = 0,1,2,3,\ldots, \mathrm{M},$$

$$\tau^n = (n-1)\Delta\tau; \qquad n = 1,2,3,4,\ldots, \mathrm{O},$$

where $i, j$, and $n$ are the space and time indices. The following is the central difference scheme for each spatial derivative:

$$\frac{\partial u_y}{\partial y} \approx \frac{(u_y)^n_{i,j+1} - (u_y)^n_{i,j-1}}{2\Delta y},$$

$$\frac{\partial u_y}{\partial x} \approx \frac{(u_y)^n_{i+1,j} - (u_y)^n_{i-1,j}}{2\Delta x},$$

$$\frac{\partial^2 u_y}{\partial x^2} \approx \frac{(u_y)^n_{i+1,j} - 2(u_y)^n_{i,j} + (u_y)^n_{i-1,j}}{(\Delta x)^2},$$

$$\frac{\partial^2 u_y}{\partial y^2} \approx \frac{(u_y)^n_{i,j+1} - 2(u_y)^n_{i,j} + (u_y)^n_{i,j-1}}{(\Delta y)^2},$$

which is the second-order central difference in space.

To get the first-order time derivative at a point $(x_i, y_j, \tau^n)$, we used the forward difference approximation as follows:

$$\frac{\partial u_y}{\partial \tau} \approx \frac{(u_y)^{n+1}_{i,j} - (u_y)^n_{i,j}}{\Delta\tau}.$$

With the help of the discretization methods, the axial velocity from (7) at $0 \le x \le 1$ becomes

$$\Rightarrow (u_y)^{n+1}_{i,j} = (u_y)^n_{i,j}\left[1 - \frac{2\Delta\tau}{Re\cdot(\Delta x)^2} - \frac{2\Delta\tau}{Re\cdot(\Delta y)^2} - S_m p_l \Delta\tau\right] - \frac{\Delta\tau}{\varepsilon.2\Delta x}\left[(u_x)^n_{i,j}(u_y)^n_{i+1,j} - (u_x)^n_{i,j}(u_y)^n_{i-1,j}\right]$$
$$- \frac{\Delta\tau}{\varepsilon.2\Delta y}\left[(u_y)^n_{i,j}(u_y)^n_{i,j+1} - (u_y)^n_{i,j}(u_y)^n_{i,j-1}\right] + \frac{\Delta\tau}{Re.(\Delta y)^2}\left[(u_y)^n_{i,j+1} + (u_y)^n_{i,j-1}\right] + \varepsilon a_0 \sin\left(\frac{\omega\tau R}{u_0}\right)\Delta\tau$$
$$+ (u_y)^n_{i+1,j}\left[\frac{\Delta\tau}{Re.(\Delta x)^2} + \frac{\Delta\tau}{Re.x.2\Delta x}\right] + (u_y)^n_{i-1,j}\left[\frac{\Delta\tau}{Re.(\Delta x)^2} - \frac{\Delta\tau}{Re.x.2\Delta x}\right] + S_m p_l (v_y)^n_{i,j}\Delta\tau - \frac{\varepsilon\Delta\tau}{D_a.Re}(u_x)^n_{i,j}, \tag{9}$$

which is the FTCSCS scheme for axial velocity of air particles,

$$\Rightarrow (v_y)^{n+1}_{i,j} = \left(1 - \frac{S_m\Delta\tau}{m}\right)(v_y)^n_{i,j} + \frac{S_m\Delta\tau}{m}(u_y)^n_{i,j}$$
$$- \frac{\Delta\tau}{2\Delta x}(v_x)^n_{i,j}\left[(v_y)^n_{i+1,j} - (v_y)^n_{i-1,j}\right]$$
$$- \frac{\Delta\tau}{2\Delta y}(v_y)^n_{i,j}\left[(v_y)^n_{i,j+1} - (v_y)^n_{i,j-1}\right], \tag{10}$$

which is the FTCSCS scheme for the axial velocity of dust particles.

Following stability criteria, the accuracy of the results is verified, and it is discovered that the results converge to a certain degree,[21]

$$\mathrm{Max}\left\{\frac{\Delta\tau}{\Delta x^2}\right\} \le 0.5, \tag{11}$$

where $\nabla\tau = 4\times10^{-6}$ and $\nabla x = 0.003$ are taken.

## III. RESULTS AND DISCUSSION

Our goal in this work was to use a two-dimensional pulsatile flow regime to determine the velocity profile of air and dust particles as well as the impact of lung porosity on the deposition of nanoparticles by varying Reynolds number between ($10 \le Re \le 20$) and Darcy number ($0.001 \le Da \le 0.1$). The following parameter values have been used in numerical calculations: R = 0.5 mm, $m$ = 0.0002 gm, $d_p$ = 50 nm, $f$ = 1.2 Hz $\nabla\tau = 4\times10^{-6}$, $\nabla x = 0.003$, $\nabla y = 0.006$, $\upsilon = 1.655\times10^{-5}$ m$^2$ s$^{-1}$, $a_0 = 1$ kg/m$^2$ s$^2$, $\rho_a = 1.145$ kg/m$^3$, $\rho_p = 0.025\,04\times10^{12}$ m$^{-3}$, Re = 10–20, $\varepsilon = 0.6$, $\mu = 1.895\times10^{-5}$ kgm$^{-1}$ s$^{-1}$.[20,24–26]

The mesh is a grid of points (nodes) that divides the area of interest into discrete elements, allowing for numerical simulations of fluid dynamics. Our mesh is generated for the grid size 151 × 201 with 2000 nodes for time. Figure 3 shows that due to alveolar expansion, some inspired air moves axially to the distal airways during inhalation, while the remaining inspired air moves radically, as seen in Fig. 3. We saw that the axial and radial velocity profiles of the air and dust particles are parabolic. For the flow field and aerosol deposition, such a mesh size proved to provide precise answers.

Figures 4(a) and 4(b) show schematic diagrams of the airflow and dust flow, respectively, in the respiratory bronchial tube. When the inspiratory flow increases, the deposition increases for all particle sizes. The color bar on the right side of the figure stands for the measurement of the velocity of the flow field of the tube.

We saw from contour Figs. 4(a) and 4(b) that the velocity of air and dust particles decreases with distance. There is a maximum

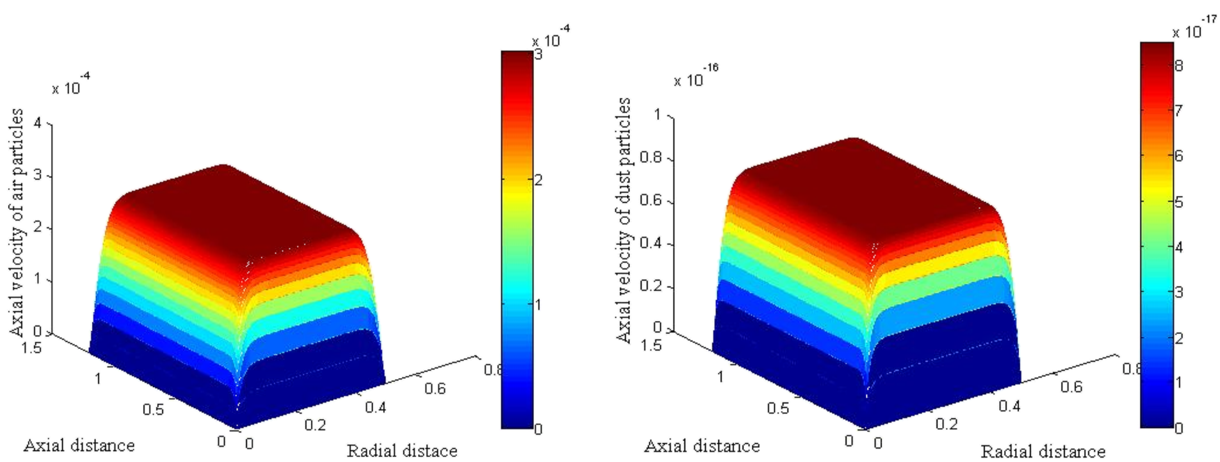


(a) (b)

FIG. 3. Mesh for axial velocity of (a) air particles and (b) dust particles.

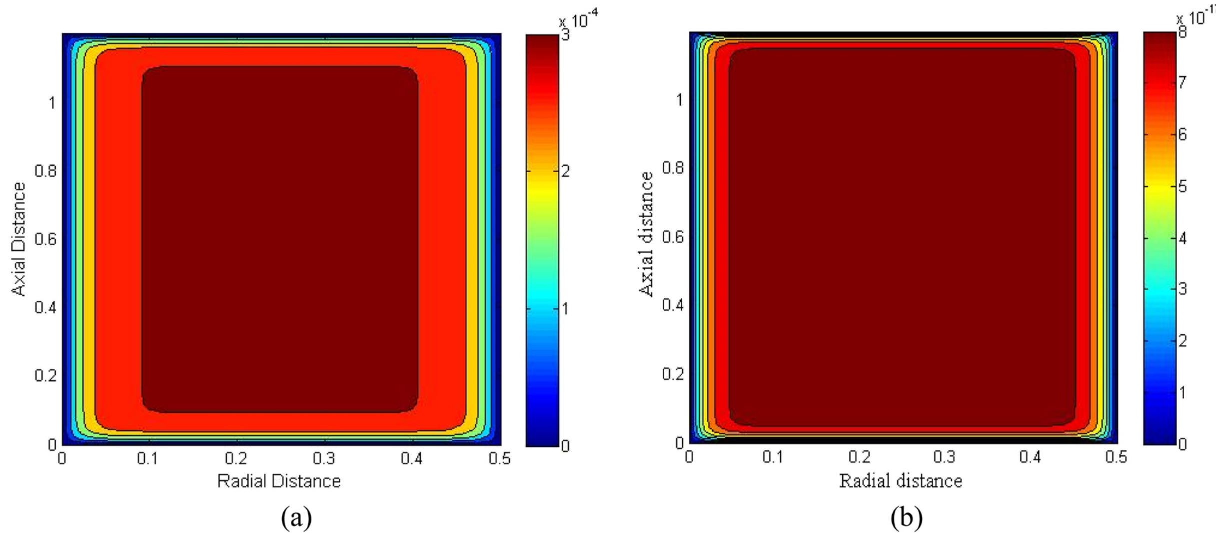


**FIG. 4.** The contour of (a) air particles and (b) dust particles.

velocity for both the air and the dust particles on the tube's axis and a minimum along the radius.

The curve visible by the red line in Figs. 5(a) and 6(a) shows the velocity profile of air and dust particles for the $x$ = 125th position in the radial direction and green, magenta, black, and blue colors for other positions in the radial direction. Similarly, the curve is visible by the red line in Figs. 5(b) and 6(b), showing the velocity profile of air and dust particles for the $y$ = 170th position along the tube and so on. We found that velocity decreases with distance.

The Darcy number in fluid dynamics through porous media represents the relative effect of the medium's permeability relative to its cross-sectional area. Since the lung is assumed to be a porous medium, the porous layer is viewed as less permeable for small values of $D_a$, while due to an increment in $D_a$, permeability increases.

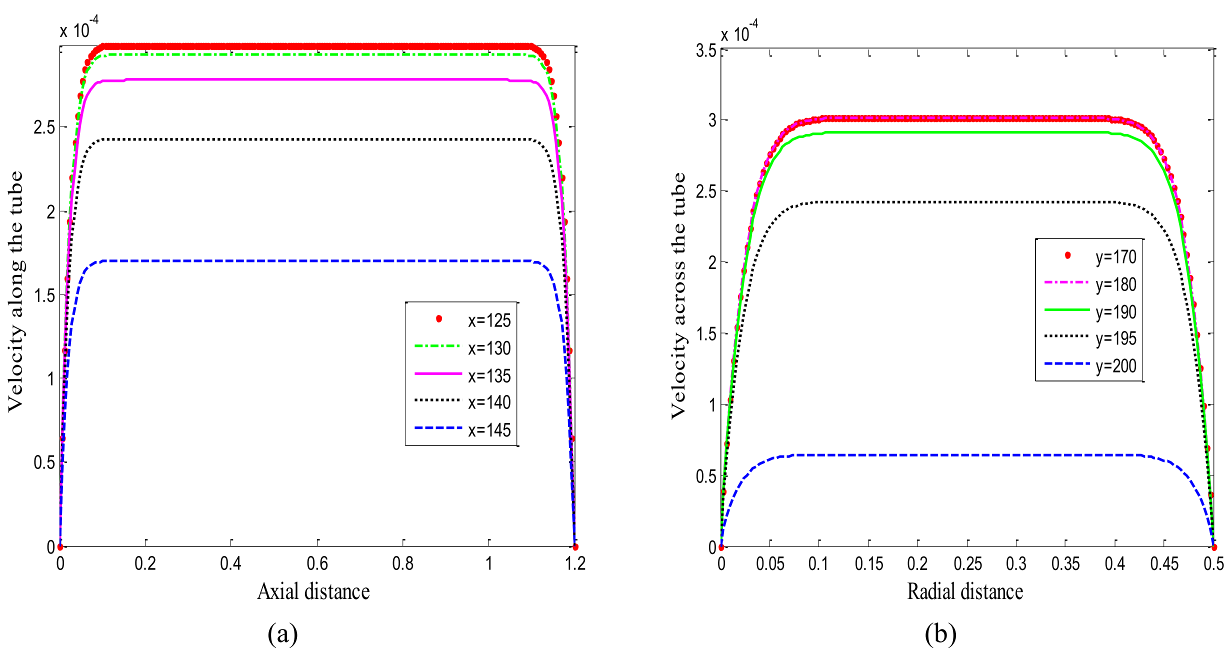


**FIG. 5.** Axial velocity of air particles (a) along the tube and (b) across the tube.

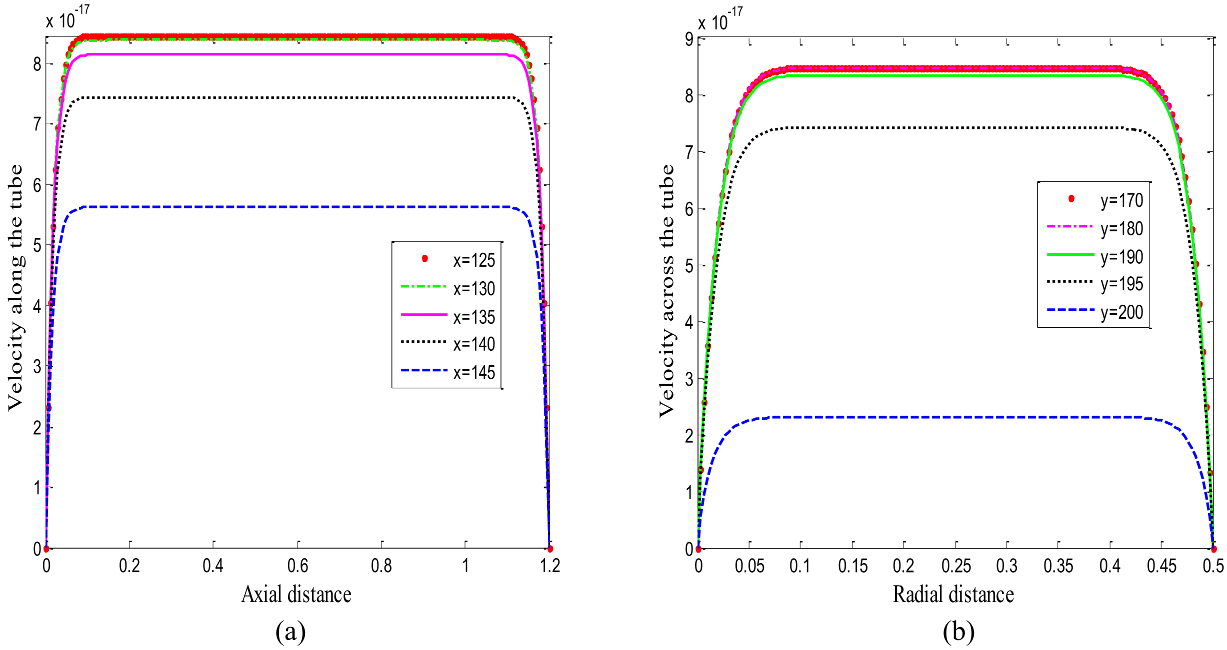


**FIG. 6.** Axial velocity of dust particles (a) along the tube and (b) across the tube.

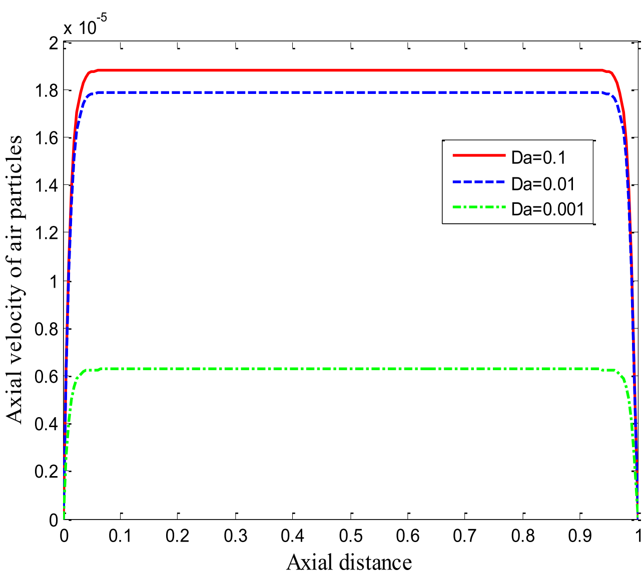


**FIG. 7.** Impact of Darcy number on air particle's axial velocity.

We discovered that the velocity of air particles has a parabolic shape for all values between 0.001 and 0.1, as illustrated in Fig. 7 permeability rises and medium pressure falls with increasing Darcy number. As a result, dust and air particles' velocities steadily rise with distance, enabling the particles to enter the lungs deeply.

The dimensionless Reynolds number is used to identify whether a channel's flow pattern is laminar or turbulent. It represents the balance between inertial and viscous forces in the airflow. We get the Reynolds number Re = 10 for $u_0 = 0.331\ \mathrm{ms}^{-1}$, $\upsilon = 1.655 \times 10^{-5}\ \mathrm{m}^2\ \mathrm{s}^{-1}$, and $\mathrm{R} = 0.5 \times 10^{-3}$ m. By varying the Reynolds number from 10 to 20 as shown in Fig. 8, we found the velocity profile for air particles in the axial direction, which shows a developing parabolic profile. Due to the fluid's pulsatile nature or

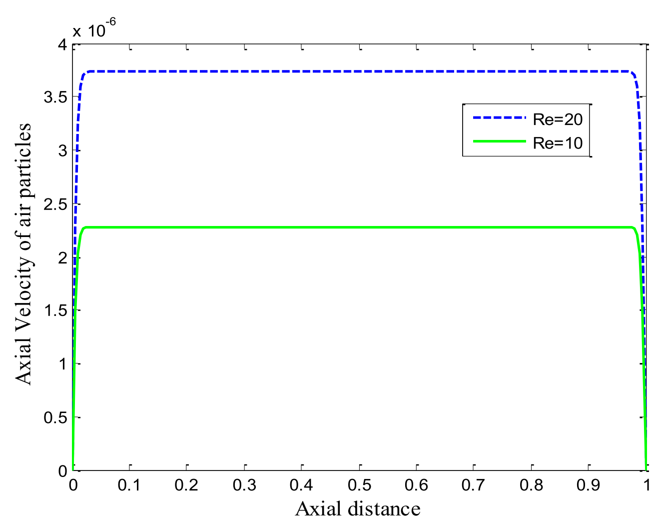


**FIG. 8.** Reynolds number impact on air particle's axial velocity.

the random movement of particles and viscosity, the velocity profile decreases as the Re gradually decreases.

## IV. CONCLUSIONS

The size of the particle determines how it is distributed throughout the lung airways. Particles smaller than those of larger sizes are spread uniformly. In this work, we study the inhalation and deposition of nanoparticles into the respiratory bronchiole via a circular tube, from which alveolar regions originate and whose walls are porous. Therefore, the following conclusions are reached after the governing equations are solved:

1. Based on our velocity profile analysis, we observed that the velocity of dust particles is lower than that of air particles. Because the density of dust particles ($\rho_p = 0.025\,04 \times 10^{12}$ $m^{-3}$) is higher than the density of air particles ($\rho_a = 1.145$ $kg/m^3$). In a flow with suspended particles, an increase in particle density often results in a change in the velocity profile of the fluid. Higher concentrations can lead to reduced velocity in regions where particles are densely packed.
2. Analysis of Darcy numbers is used to examine the flow conditions inside respiratory bronchioles. If the Darcy number increases, the media becomes more fluidic. When $D_a$ is maximized, the greatest number of particles moves in the direction of the deep lung. Relatively high Darcy numbers (more porous lung tissue) can allow nanoparticles to penetrate more readily deeper, enhancing deposition in the alveoli. Prolonged exposure to nanoparticles may lead to oxidative stress, chronic inflammation, and increased risks for cardiovascular diseases, as nanoparticles are more likely to translocate into the bloodstream.
3. Various fluid flow situations can be predicted with the help of the Reynolds number. In the respiratory tract, a low Reynolds number signifies laminar (smooth) airflow, common in smaller airways, while a higher Reynolds number indicates turbulent (chaotic) flow, often in larger airways. When comparing the results at Re = 10 with those at Re = 20, it becomes evident that the viscous forces overwhelmingly control the fluid velocity at the lower Reynolds number.

Finally, the numerical simulation of this work may provide information on the lung condition so that various lung diseases can be treated efficiently.

## AUTHOR DECLARATIONS

### Conflict of Interest

The authors have no conflicts to disclose.

### Author Contributions

**Mst. Sathi Akter**: Conceptualization (equal); Investigation (equal); Methodology (equal); Writing – original draft (equal). **Mahtab U. Ahmmed**: Supervision (equal); Writing – review & editing (equal). **Nilufer Yesmin Tanisa**: Supervision (equal); Writing – review & editing (equal). **Shakib Hossain**: Writing – review & editing (equal).

## DATA AVAILABILITY

Data sharing is not applicable to this article as no datasets were generated or analyzed during the current study.

## REFERENCES


[1] J. Heyder, "Deposition of inhaled particles in the human respiratory tract and consequences for regional targeting in respiratory drug delivery," Proc. Am. Thorac. Soc. **1**(4), 315–320 (2004).

[2] I. Manisalidis, E. Stavropoulou, A. Stavropoulos, and E. Bezirtzoglou, "Environmental and health impacts of air pollution: A review," Front. public health **8**, 14 (2020).

[3] P. G. Koullapis, S. C. Kassinos, M. P. Bivolarova, and A. K. Melikov, "Particle deposition in a realistic geometry of the human conducting airways: Effects of inlet velocity profile, inhalation flowrate and electrostatic charge," J. Biomech. **49**(11), 2201–2212 (2016).

[4] Y. Jin, X. Chen, Y. Feng, Z. Jia, J. Zhang, X. Xie, and Y. Zhang, "A novel experimental approach to measure nebulized droplet deposition pattern and deposition fraction in an idealized mouth-to-throat model," Phys. Fluids **35**(8), 083322 (2023).

[5] Y. D. Shang, K. Inthavong, and J. Y. Tu, "Detailed micro-particle deposition patterns in the human nasal cavity influenced by the breathing zone," Comput. Fluids **114**, 141–150 (2015).

[6] D. K. Sleeth, S. A. Balthaser, S. Collingwood, and R. R. Larson, "Estimation of the human extrathoracic deposition fraction of inhaled particles using a polyurethane foam collection substrate in an IOM sampler," Int. J. Environ. Res. Public Health **13**(3), 292 (2016).

[7] J. Löndahl, W. Möller, J. H. Pagels, W. G. Kreyling, E. Swietlicki, and O. Schmid, "Measurement techniques for respiratory tract deposition of airborne nanoparticles: A critical review," J. Aerosol Med. Pulm. Drug Delivery **27**(4), 229–254 (2014).

[8] C. A. Ruge, J. Kirch, O. Cañadas, M. Schneider, J. Perez-Gil, U. F. Schaefer, C. Casals, and C. M. Lehr, "Uptake of nanoparticles by alveolar macrophages is triggered by surfactant protein A," Nanomed. Nanotechnol. Biol. Med. **7**(6), 690–693 (2011).

[9] H. R. Paur, F. R. Cassee, J. Teeguarden, H. Fissan, S. Diabate, M. Aufderheide, W. G. Kreyling *et al.*, "In-vitro cell exposure studies for the assessment of nanoparticle toxicity in the lung—A dialog between aerosol science and biology," J. Aerosol Sci. **42**(10), 668–692 (2011).

[10] L. Morawska, W. Hofmann, J. Hitchins-Loveday, C. Swanson, and K. Mengersen, "Experimental study of the deposition of combustion aerosols in the human respiratory tract," J. Aerosol Sci. **36**(8), 939–957 (2005).

[11] H. Qiao, W. Liu, H. Gu, D. Wang, and Y. Wang, "The transport and deposition of nanoparticles in respiratory system by inhalation," J. Nanomater. **2015**(1), 394507.

[12] D. B. Kwak, S. C. Kim, H. Lee, and D. Y. Pui, "Numerical investigation of nanoparticle deposition location and pattern on a sharp-bent tube wall," Int. J. Heat Mass Transfer **164**, 120534 (2021).

[13] M. E. Taghavizadeh Yazdi, M. Qayoomian, S. Beigoli, and M. H. Boskabady, "Recent advances in nanoparticle applications in respiratory disorders: A review," Front. Pharmacol **14**, 1059343 (2023).

[14] W. Hofmann, R. Golser, and I. Balashazy, "Inspiratory deposition efficiency of ultrafine particles in a human airway bifurcation model," Aerosol Sci. Technol. **37**, 988–994 (2003).

[15] A. Saini and V. K. P. Katiyar, "Effects of first-order chemical reactions on the dispersion coefficient associated with laminar flow through the lungs," Int. J. Biomath. **07**(2), 1450021 (2014).

[16] H. Shi, C. Kleinstreur, Z. Zhang, and C. S. Kim, "Nanoparticle transport and deposition in bifurcating tubes with different inlet conditions," Phys. Fluids **16**, 2199–2213 (2004).

[17] J. X. Xi and P. W. Longest, "Effects of oral airway geometry characteristics on the diffusional deposition of inhaled nanoparticles," J. Biomech. Eng. **130**(1), 0110081 (2008).

[18]Z. Zhang and C. Kleinstreuer, "Airflow structures and nano-particle deposition in a human upper airway model," J. Comput. Phys. **198**, 178–210 (2004).
[19]Z. Zhang, C. Kleinstreurer, J. F. Donohue, and C. S. Kim, "Comparison of micro- and nano-size particle depositions in a human upper airway model," J. Aerosol Sci. **36**, 211–233 (2005).
[20]A. Saini, V. K. Katiyar, and Pratibha, "Two-dimensional model of nanoparticle deposition in the alveolar ducts of the human lung," Appl. Appl. Math. **12**, 305–318 (2017).
[21]J. Kori and Pratibha, "Numerical simulation of dusty air flow and particle deposition inside permeable alveolar duct," Int. J. Appl. Comput. Math **5**(1), 17 (2019).
[22]S. Ergun, "Fluid flow through packed columns," Chem. Eng. Prog. **48**, 89–94 (1949).
[23]K. Vafai, "Convective flow and heat transfer in variable-porosity media," J. Fluid Mech. **147**, 233–259 (1984).
[24]Z. Ismail, I. Abdullah, N. Mustapha, and N. Amin, "A power-law model of blood flow through a tapered overlapping stenosed artery," Appl. Math. Comput. **195**, 669–680 (2008).
[25]J. N. Kapur, *Mathematical Models in Biology and Medicine* (East-West Press Pvt. Ltd., New Delhi, 1985).
[26]P. K. Mandal, "An unsteady analysis of non-Newtonian blood flow through tapered arteries with a stenosis," Int. J. Non-Linear Mech. **40**, 151–164 (2005).